Research Article

Mohamed Elhag*, Jarbou Bahrawi, and Silvena Boteva

# Input/output inconsistencies of daily evapotranspiration conducted empirically using remote sensing data in arid environments

https://doi.org/10.1515/geo-2020-0141
received May 10, 2020; accepted February 22, 2021

**Abstract:** The reliable quantification of daily evapotranspiration (ET) over vast croplands is a quest in many scholarly works aimed at the precise practice of water resources management. Remote sensing–based empirical and nonempirical models were developed to overcome large-scale quantification issues, which are usually experienced when using conventional approaches for the estimation of ET. The surface energy balance system (SEBS) model was used to quantify the daily ET in the arid/semi-arid over Wadi Ad-Dwaser, Saudi. SEBS input variables are parametrically sensitive and climatic dependent, and the model input/output dependencies are of high comprehensibility; therefore, the optimization analysis of SEBS input/output parameters is the target of the current research. SEBS inputs reciprocal inconsistencies were determined using the artificial neural network analysis, while the output dependencies on the daily ET estimation were mapped. Results demonstrated that the temperature and relative humidity are the most sensitive parameters to be considered in the routine crop monitoring procedure. SEBS output thematic maps showed the robust proportional correlation between the daily ET and the conducted temperature map. Moreover, the estimated daily ET was inversely correlated with the estimated cold sensible heat fluxes. The findings suggest systematic monitoring and forecasting procedures for efficient water-saving management plans in Saudi Arabia.

**Keywords:** daily evapotranspiration, desirability function, neural network analysis, SEBS

## 1 Introduction

The estimation of daily evapotranspiration (ET) using the remote sensing data was successfully applied to the last decade of agricultural studies. The remote sensing data were continuously developed and improved to enclose the far-infrared and short-wave infrared as crucial segments of the electromagnetic spectrum [1,2]. The latter two segments showed extensive importance in water-related scholarly studies rather in atmospheric water studies at the top of atmosphere level [3,4] or at the top of canopy (TOC) level [5,6]. The TOC applications of remote sensing covered the soil/water relationships as well as the water/crop relationships [7,8].

The substantial quantification of the ET exploiting remote sensing imagery proved significantly the quantum involvement of the sensible heat fluxes interacted with the TOC water vapor in large-scale agricultural practices [9,10]. Nevertheless, the implementation of the adopted algorithms is valid solely in local-scale practices, while the large-scale agricultural practices are used to encounter droughts due to the interactions of surface geometry and heat flux fluctuation, besides the lack of meteorological data consistency [11,12].

Empirical and nonempirical algorithms to quantify the daily ET were lately developed to serve purposes and different spatial configuration settings [13,14]. Those physical models were heavily dependent on the physical parameters of the surrounding environments, and therefore, the biological parameters were less involved [15,16]. The most recently developed algorithms to quantify the

* **Corresponding author: Mohamed Elhag,** Department of Hydrology and Water Resources Management, Faculty of Meteorology, Environment and Arid Land Agriculture, King Abdulaziz University, Jeddah, 21589, Saudi Arabia; Institute of Remote Sensing and Digital Earth (RADI), Chinese Academy of Science (CAS), Beijing, 100094, China; Department of Applied Geosciences, Faculty of Science, German University of Technology in Oman, Muscat 1816, Oman, e-mail: melhag@kau.edu.sa
**Jarbou Bahrawi:** Department of Hydrology and Water Resources Management, Faculty of Meteorology, Environment and Arid Land Agriculture, King Abdulaziz University, Jeddah, 21589, Saudi Arabia
**Silvena Boteva:** Department of Ecology and Nature Conservation, Faculty of Biology, Sofia University "St. Kl. Ohridski", 8 Dragan Tsankov Blvd, 1164 Sofia, Bulgaria

daily ET showed the synergy between the physical and the biological parameters in a single biophysical algorithm performance [17–20].

One of the current and best-performing calculations to estimate ET is the semi-empirical SEBS model founded by Su [21]. SEBS considers not only a diverse range of land surfaces but also the physical and biological parameters that were conducted from two European Space Agency sensors: Advanced Along-Track Scanning Radiometer (AATSR) and MEdium Resolution Imaging Spectrometer (MERIS) symbolism.

Optimization analysis could convey a significant determination to the hesitation in multi-input measurement uncertainties. It is a functional strategy to analyze the intuitive relationship between detached frameworks [23]. The optimization analysis procedures and its executions are discussed in the studies by Ficici et al. [24] and Kunnan and Carr [25]. The procedure of the comprehensive study generally examines the most extreme, least, and the mean desirability parameters for singular observations considering the reality that the desirability analysis and its transformations led to a forecasted retort into nonscaled values [26–28].

The artificial neural network (ANN) analysis was developed by Jo et al. [29]. The back-propagation method was the conceptual development of ANN to be implemented extensively after [30] the neural network training procedure. The uses of ANN are comprehensively and successfully applied in several fields related to hydrology and water resources management. Related fields to water quality assessment and water resources management were discussed in the previous studies [31–35].

The objectives of the research are the realization of the SEBS algorithm over a large-scale agricultural practice in an arid environment and then to thematically map SEBS outputs. Consequently, an optimization analysis of SEBS input parameters will be exercised to comprehend SEBS inputs reciprocal inconsistencies using the ANN analysis. Finally, the SEBS model output dependencies are assessed against the estimated ET over Wadi Ad-Dwaser, Saudi Arabia.

## 2 Materials and methods

### 2.1 Study area

Wadi Adwaser is a typical example of an arid environment located in Saudi Arabia. Wadi Adwaser is located at 44°43′ latitude and 20°29′ longitude, which is at an approximate distance of 600 km southwest of Riyadh, the capital city of Saudi Arabia (Figure 1). The major activity in Wadi Ad-Dwaser is agriculture. More than 1,20,000 hectares of the designated study area is used for Alfalfa crop production as a whole-year fodder [36]. The main irrigation system is the pivot sprinklers connected to water pumps. These are deep-well pumps that convey groundwater continuously to the sprinklers. The extensive use of the groundwater resources in Wadi Ad-Dwaser led to a drastic drop in the groundwater level and irrecoverable soil salinity problems [37]. The mean annual temperature in the designated study area is

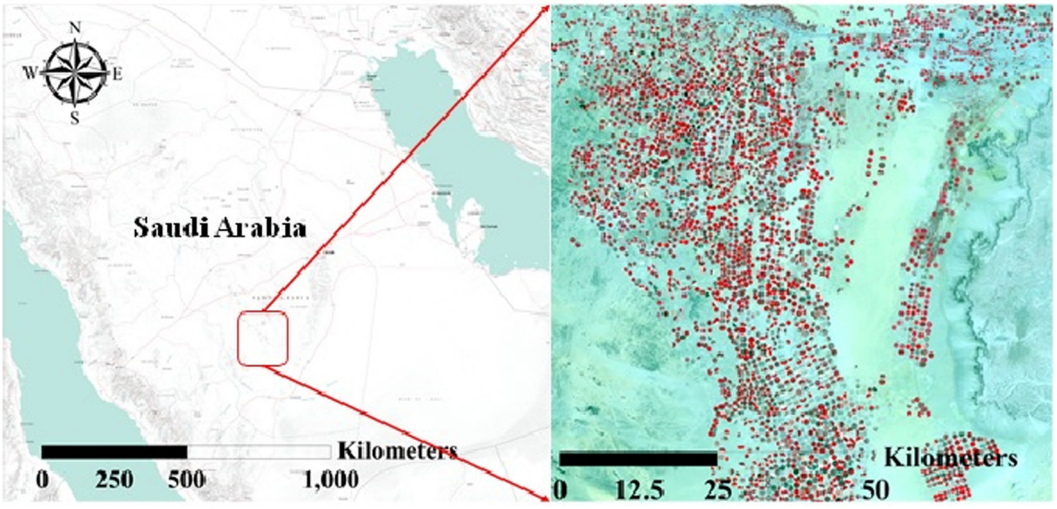


**Figure 1:** Location of the study area in a false color composite where the agricultural areas of Wadi Ad-Dwaser appear as red dots [39].

around 37°C with huge variations between the maximum temperatures of 45°C and the minimum temperature closely to 3°C. The mean annual rainfall is reported to be less than 18 mm with mostly sunny day's long solar radiation [38].

## 2.2 Data sets

The use of the SEBS calculation necessitates input parameters from four remote sensing images that can be acquired from three unique informational collections: (1) two datasets of AATSR images acquired in March and June 2012, (2) two datasets of MERIS images acquired in synchronization with the AATSR images and the total number of the remote sensing datasets is four images, and (3) meteorological data, as entirely mentioned in the studies by Su [18] and Elhag et al. [10]. The meteorological data utilized in the current study are incorporated in the form of 10-year monthly average temperature, relative humidity, wind speed, and solar radiation to ensure the meteorological stability of the used data [22,40]. The information was gathered amid August 2012 (Table 1).

## 2.3 The SEBS fundamentals

SEBS comprises a sequence of examination practices for the assurance of the surface physical and biophysical parameters to be initially assessed. These parameters are albedo, emissivity factor, maximum and minimum temperature, and vegetation possibilities. Finally, a model for the assurance of the evaporative fraction estimation based on meteorological restriction conditions to the wet/dry weather limit was adopted [18]. The SEBS essential conditions are as follows:

$$Rn = G_0 + H + \lambda \times E, \tag{1}$$

where $Rn$ is the net radiation (watt/m$^2$), $G_0$ is the soil heat flux (watt/m$^2$), $H$ is the turbulent sensible heat flux (watt/m$^2$), $\lambda E$ is the turbulent latent heat flux (watt/m$^2$), and $H$ is the actual sensible heat flux (watt/m$^2$).

The pixel conditions representing the dry ($H$-dry) and the wet ($H$-wet) metrological settings are controlled by the actual sensible heat fluxes. The $H$-dry and the $H$-wet pixel values are determined by equation sequence under the hypothesis of having a comprehensive wet condition [10]. Therefore, the daily ET estimation ($E_{\text{daily}}$) is estimated as follows:

$$E_{\text{daily}} = \underset{24}{\overset{0}{\Lambda}} \times 8.64 \times 10^7 \times \frac{Rn - G_0}{\lambda \rho_\omega}, \tag{2}$$

where $\Lambda_{24}^{0}$ is the anticommutative exterior product of daily evaporative fraction, $\rho_\omega$ is the density of water kg/m$^3$, $\lambda$ is the latent heat of vaporization (watt/m$^2$), and $E$ is the actual evaporation (mm/day).

A total number of 52 ground truth standardized Penman–Monteith ET data were collected uniformly to verify the daily ET conducted in the current study using an SEBS model. The lysimeter technique was carried out according to Liu and Wang [41] with ±0.025 calibrated accuracy. The calibration procedure was principally based on placing double infiltrometers of Taylor [42].

**Table 1:** Meteorological data of 10-year monthly average used to empower SEBS model

| Month | Minimum temperature (°C) | Maximum temperature (°C) | Humidity (%) | Wind (km/day) | Sun expo. (h) | Radiation (MJ/m²/day) |
|---|---|---|---|---|---|---|
| January | 3.7 | 25.2 | 40 | 346 | 7.4 | 15.7 |
| February | 5.8 | 28.6 | 34 | 302 | 8.2 | 18.5 |
| March | 9.4 | 32.9 | 28 | 302 | 8.7 | 21.3 |
| April | 12.8 | 37.9 | 27 | 302 | 8.9 | 23.0 |
| May | 17.8 | 42.8 | 16 | 302 | 7.1 | 20.6 |
| June | 19.8 | 45.1 | 11 | 259 | 8.1 | 22.0 |
| July | 21 | 45.5 | 13 | 346 | 6.5 | 19.6 |
| August | 25.1 | 45.4 | 13 | 302 | 6.3 | 19.1 |
| September | 17.5 | 42.8 | 15 | 259 | 7.7 | 20.2 |
| October | 12.5 | 37.7 | 21 | 216 | 7.8 | 18.5 |
| November | 7.5 | 31.1 | 29 | 259 | 8.5 | 17.4 |
| December | 4.9 | 26.5 | 37 | 216 | 6.6 | 14.1 |
| Average | 13.1 | 36.8 | 24 | 284 | 7.6 | 19.2 |

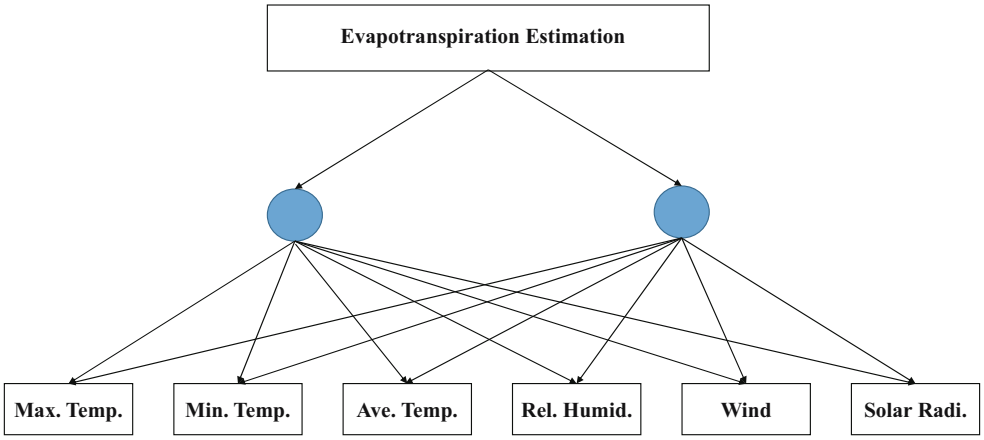


**Figure 2:** The outline of the ANN analysis including one hidden layer and two nodes.

## 2.4 Optimization function analysis

The reason for utilizing the optimization analysis is to simultaneously enhance the model forecasts considering numerous conditions. Optimization analysis is a standout practice found among the most well-known methodologies used to expand a few progressions of response [23]. In a general sense, the desirability analysis changes over the information capacities into (0,1) scale to enhance the model forecasting in terms of optimization. Derringer and Suich [23] reported that the optimization analysis is based on three procedural approaches.

Maximization analysis:

$$d_r^{\max} = \begin{cases} 0 & \text{if } f_{r(X)} < A \\ \left(\dfrac{f_r(X) - A}{B - A}\right)^s & \text{if } A \le f_{r(X)} \le B \\ 1 & \text{if } f_{r(X)} > B. \end{cases} \tag{3}$$

Minimization analysis:

$$d_r^{\min} = \begin{cases} 0 & \text{if } f_{r(X)} > B \\ \left(\dfrac{f_r(X) - B}{A - B}\right)^s & \text{if } A \le f_{r(X)} \le B \\ 1 & \text{if } f_{r(X)} < A. \end{cases} \tag{4}$$

Overall desirability:

$$d_r^{\text{target}} = \begin{cases} \left(\dfrac{f_r(X) - A}{t_0 - A}\right)^s & \text{if } A \le f_{r(X)} \le t_0 \\ \left(\dfrac{f_r(X) - B}{t_0 - B}\right)^s & \text{if } t_0 \le f_{r(X)} \le B \\ 0 & \text{Otherwise,} \end{cases} \tag{5}$$

where $A$, $B$, and $S$ are the analysis scope of the predefined variables, high $f(X)$ is the higher desirability, and low $f(X)$ is the low desirability. The three parametric optimization settings are with the exact scale and periodic at the given points $A$, $B$, and $t_0$.

## 2.5 ANN concepts

The ANN analysis was implemented in the current study to decompose the interconnected relationships of the input parameters for the better comprehensive standing of the problem. In this study, the neural analysis was carried out based on the study by Monahan [43].

The neural network regression method can be conducted as follows:

$$Y = \alpha + \sum_h w_h \phi_h \left(\alpha_h + \sum_{i=1}^{p} w_{ih} X_i\right), \tag{6}$$

where $Y = E(Y|X)$ and $Y$ is the final neuron output value, $w$ is the assigned weight between the nodes, $X$ is the assigned value of the nodes, and $\phi_h$ is the activation function.

Such neural network settings can function under only one hidden layer to avoid the model overfitting [44]. The $\phi(z)$ function implemented in the current ANN is a hyperbolic refraction stimulation function. It is implemented for the logistic stimulation of the hidden layers.

$$\phi(z) = \tanh(z) = \frac{1 - e^{-2z}}{1 + e^{-2z}}. \tag{7}$$

To limit the model predictions between 0 and 1, the concluding productions must be in a linear relationship. The skip-layer diagram of the neural network analysis is shown in Figure 2.

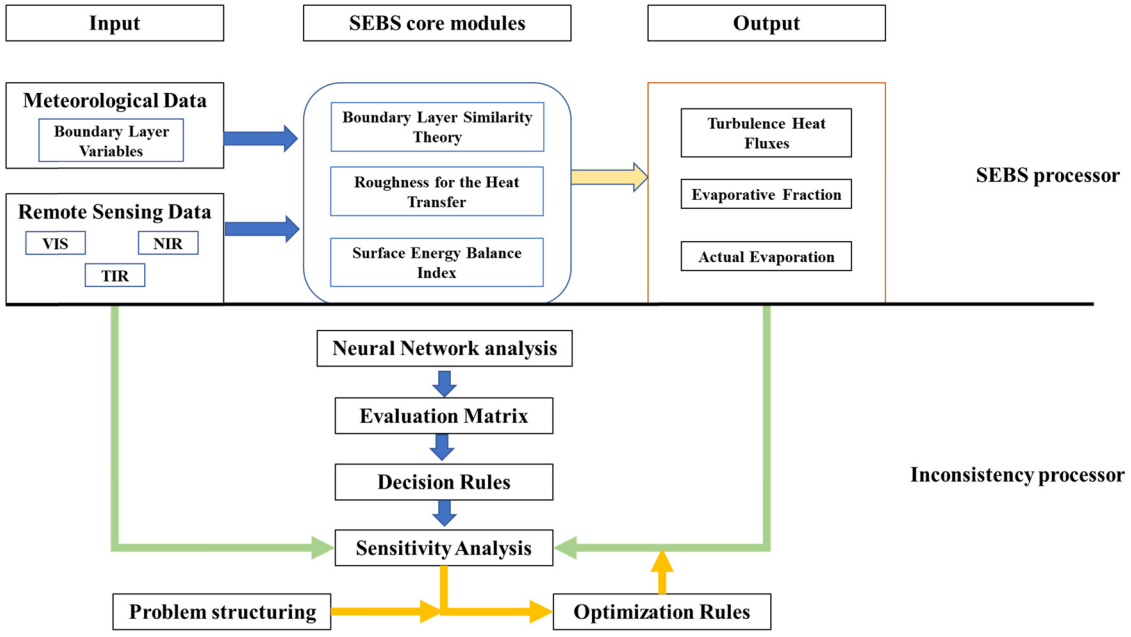


**Figure 3:** Conceptual framework scheme.

The following is the equation for the skip-layer ANN for regression:

$$Y = \alpha + \sum_{i=1}^{p} \beta_i X_i + \sum_{h} w_h \phi_h \left( \alpha_h + \sum_{i=1}^{p} w_{ih} X_i \right). \quad (8)$$

It ought to be evident that these approaches are exceedingly parameterized and subsequently will tend to overfit the investigated datasets. Cross-validation is a consequent practice to ensure that the prescient execution of the neural network analysis is satisfactory.

The skip-layer neural network analysis is conducted as follows:

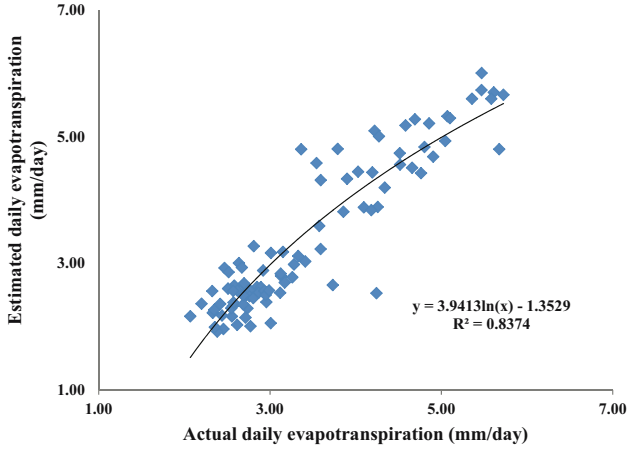


**Figure 4:** The correlation between the actual and the estimated daily ET.

$$Y = \alpha + \sum_{i=1}^{p} \beta_i X_i + \sum_{h} w_h \phi_h \left( \alpha_h + \sum_{i=1}^{p} w_{ih} X_i \right). \quad (9)$$

However, this model tends to overfit its training datasets. Therefore, assurance of the satisfactory execution of the ANNs demonstrates is an unquestionable requirement. Five distinct evaluation criteria are utilized to decide the optimum fit: the Pearson correlation coefficient of connection ($R$), the root mean square error (RMSE), the mean absolute deviation (MAD), the negative log-likelihood, and finally the unconditional sum of squares (SSE). Essentially, RMSE is the preferred analyzed parameter for comparability explanations. RMSE can be calculated as follows:

$$\text{RMSE} = \sqrt{\frac{1}{T_0} \sum_{t=1}^{T_0} (y_1 - \hat{y}_1)^2}, \quad (10)$$

where $T$ is the time index and $\hat{y}_t$ and $y_t$ iare the predicted and the actual values, respectively. Primarily, the higher value of $R$ and smaller values of RMSE are considered to ensure the improved functionality of the model.

## 2.6 Output statistical analysis

Univariate statistical analysis is performed to find mean, standard deviation, number, sum, quantile, maximum, minimum, and $N$ missing functions. These functions

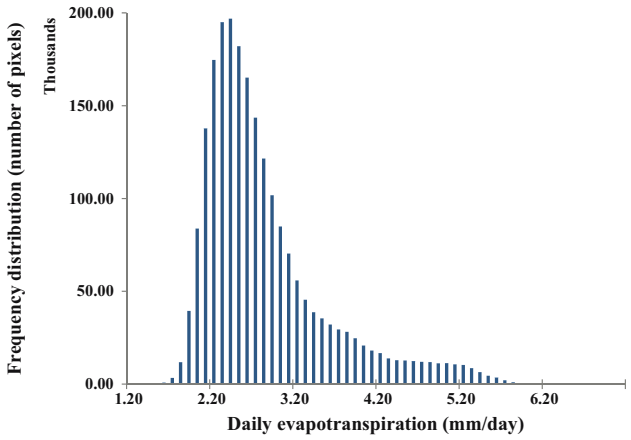


**Figure 5:** The frequency distribution of the estimated daily ET.

run across columns or rows. The statistic is computed for each row across the series of rows. The quantile function was performed to evaluate the conducted values, ascendingly in the tabulate manner, of the 2D image data from 0 to 1 according to Cheng and Parzen [45] as follows:

$$Q_{(x)} = \mathrm{Col}Q\left\{X\frac{N\mathrm{Row}(i) - N\mathrm{Row}(j)}{N\mathrm{Row}(i) - 1}\right\}. \quad (11)$$

Regression analysis was carried out to investigate the reliance of the conducted daily ET on the albedo, temperature *H*-dry, and *H*-wet outputs. The scatter plot matrix was conducted using the restricted maximum likelihood equation (RMLE) function according to the study by Robert and Gene Hwang [46] as follows:

$$-2l(\theta\,|z) = (K'z)\left(K'\sum_{\theta}K\right)^{-1}(K'z) + \log K'\sum_{\theta}K + n\,\log(2\pi), \quad (12)$$

where $K'$ has full row rank of $N$.

To understand the conceptual framework of the study under investigation, SEBS input/output diagram shown in Figure 3 indicates that the main inputs of SEBS model are meteorological data combined with certain remote sensing imagery. Conversely, the output data are mainly thermal maps where each of which is used for different data measures. The inconsistency process starts with the problem definition utilizing the collected problem-solving information. Consequently, the analysis matrix can be performed with different weights of criteria in a comparable mode [47,48]. Throughout the normalization methods, the weights were transformed into a uniform scale value between 0 and 1. The value function converts the implementation of an option into a weighted score, which represents the degree to which a decision objective is matched [49].

# 3 Results and discussion

## 3.1 SEBS realization

The application of the SEBS model over the designated study area has produced 21 different output thematic maps related to surface energy fluxes. The actual daily ET and the evaporative fraction thematic maps were demonstrated caused by their relative significance to the study purposes. According to the regression equation demonstrated in Figure 4 ($Y = 3.939\ \ln(x) - 1.4319$ and $R^2 = 0.8189$), the application of the SEBS model over the study area is significantly correlated with the ground truth data measurements collected from the lysimeter.

The idea behind drawing the best fit line assumes that the data are scattered along a line that represents the least squares regression error. This equation is of substantial sensible use because the water balance information is required for the irrigation requirements in the study area or under similar conditions. Therefore, the actual daily ET values were verified using real data *in situ* measurements.

**Table 2:** Gaussian analysis using Jackknife-predicted model

| | Jackknife predicted model | | | |
|---|---|---|---|---|
| | **Theta** | **$\mu$** | **$\sigma^2$** | **−2*log-likelihood** |
| **SEBS inputs** | | | | |
| Maximum temperature | 31.4 | 13.5 | 22.5 | 82.4 |
| Minimum temperature | 20.7 | 28.3 | 27.1 | 83.9 |
| Average temperature | 26.8 | 20.9 | 24.3 | 83.1 |
| Relative humidity | 13.6 | 0.7 | 0.0 | −30.7 |
| Wind speed | 100 | 1.3 | 0.0 | −6.7 |
| Solar radiation | 2.6 | 1957.3 | 322469.6 | 199.8 |

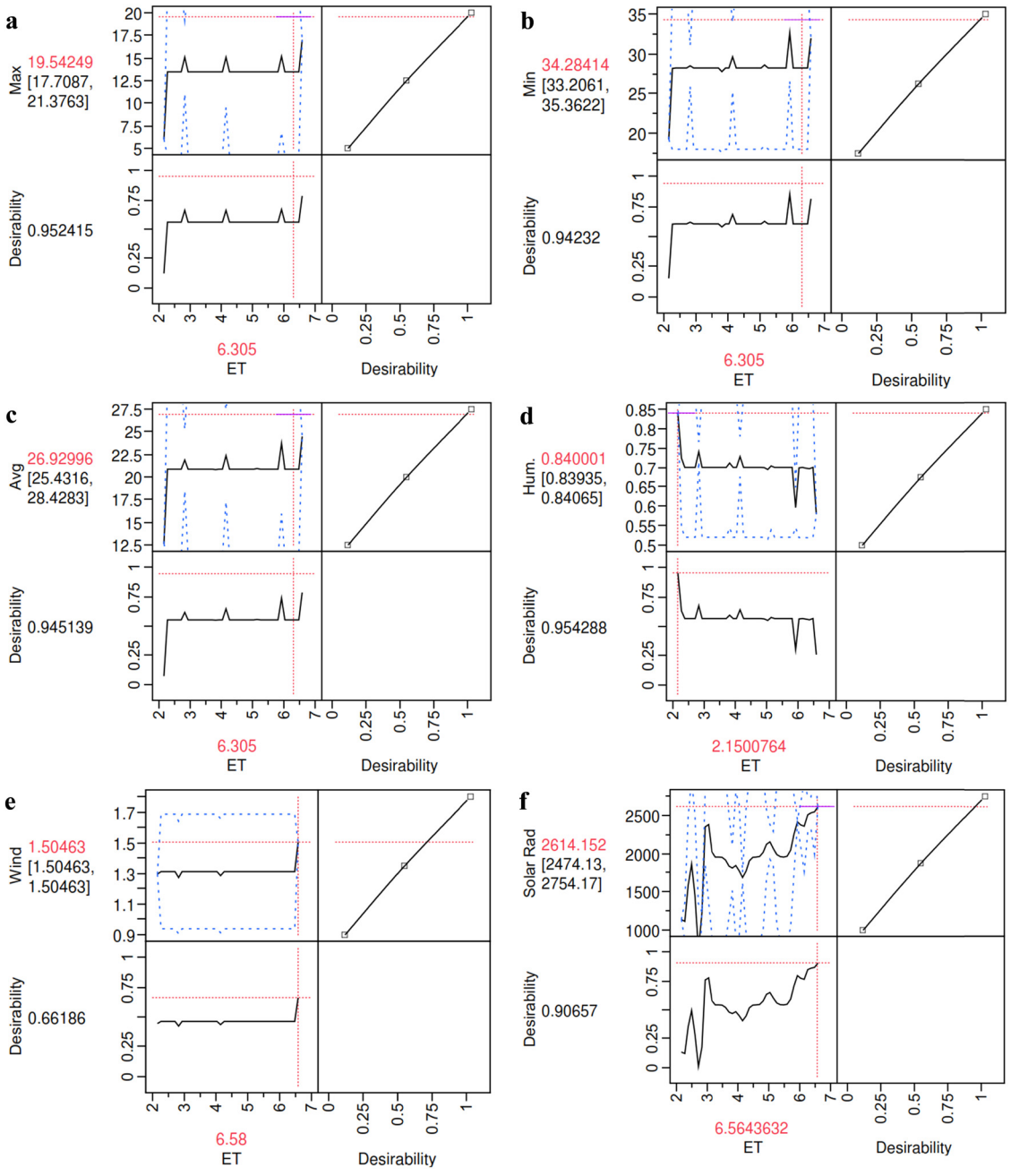


**Figure 6:** Prediction profiler of SEBS input parameters under optimization function. SEBS inputs are (a) maximum temperature, (b) minimum temperature, (c) the average temperature, (d) relative humidity, (e) wind speed, and (f) solar radiation.

Consequential information could be collected from remote sensing data only when the inadequacy conditions are considered. Inadequacy conditions for the application of the SEBS model primarily depend on the surface roughness [18], the planetary boundary layer [50], and land use land cover type [51,52].

The frequency distribution of daily ET values over the study area illustrated in Figure 5 has a mean frequency peak value at 2.4 mm, corresponding to the temperature distribution value of 322 K.

## 3.2 Input inconsistencies

Table 2 and Figure 6 show the Gaussian analysis of the Jackknife predicated model and the desirability function

**Table 3:** ANN analysis for SEBS input parameters

| | Training measures | | Validation measures | | Predication profiler |
|---|---|---|---|---|---|
| Maximum temperature | $R^2$ | 0.73244 | $R^2$ | 0.62325 | 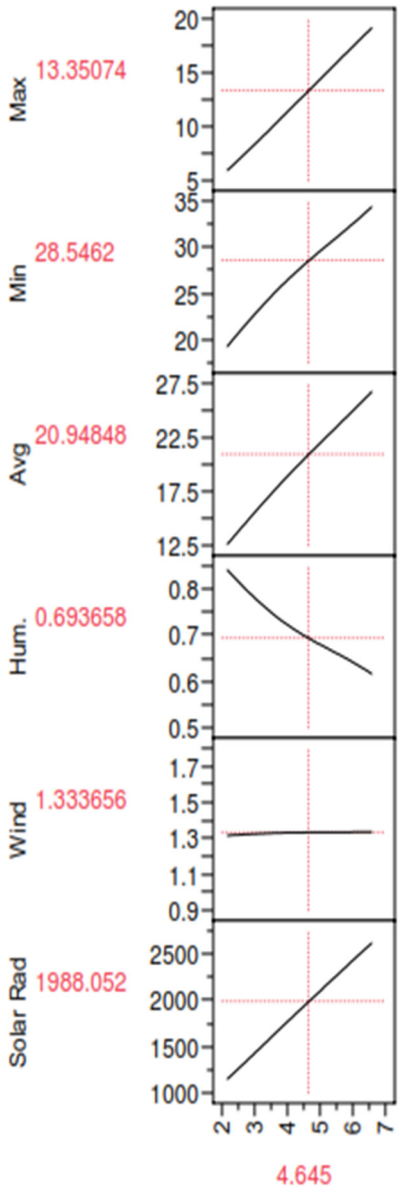 |
| | RMSE | 2.44274 | RMSE | 2.76878 | |
| | Mean absolute deviation | 2.04149 | Mean absolute deviation | 2.41238 | |
| | –log-likelihood | 20.8085 | –log-likelihood | 12.1867 | |
| | SSE | 53.7028 | SSE | 38.3308 | |
| | Sum frequency | 9 | Sum frequency | 5 | |
| Minimum temperature | $R^2$ | 0.84119 | $R^2$ | 0.84231 | |
| | RMSE | 1.95751 | RMSE | 2.09276 | |
| | Mean absolute deviation | 1.69674 | Mean absolute deviation | 1.78596 | |
| | –log-likelihood | 18.8155 | –log-likelihood | 10.7871 | |
| | SSE | 34.4865 | SSE | 21.8982 | |
| | Sum frequency | 9 | Sum frequency | 5 | |
| Average temperature | $R^2$ | 0.79173 | $R^2$ | 0.75405 | |
| | RMSE | 2.19008 | RMSE | 2.4088 | |
| | Mean absolute deviation | 1.86911 | Mean absolute deviation | 2.09916 | |
| | –log-likelihood | 19.8259 | –log-likelihood | 11.4903 | |
| | SSE | 43.168 | SSE | 29.0117 | |
| | Sum frequency | 9 | Sum frequency | 5 | |
| Relative humidity | $R^2$ | 0.83576 | $R^2$ | 0.81527 | |
| | RMSE | 0.02941 | RMSE | 0.0499 | |
| | Mean absolute deviation | 0.02292 | Mean absolute deviation | 0.0321 | |
| | –log-likelihood | –18.967 | –log-likelihood | –7.8937 | |
| | SSE | 0.00779 | SSE | 0.01245 | |
| | Sum frequency | 9 | Sum frequency | 5 | |
| Wind speed | $R^2$ | 0.00082 | $R^2$ | –0.0269 | |
| | RMSE | 0.20227 | RMSE | 0.16364 | |
| | Mean absolute deviation | 0.15755 | Mean absolute deviation | 0.14555 | |
| | –log-likelihood | –1.6130 | –log-likelihood | –1.9558 | |
| | SSE | 0.36821 | SSE | 0.13389 | |
| | Sum frequency | 9 | Sum frequency | 5 | |
| Solari radiation | $R^2$ | 0.98032 | $R^2$ | 0.98621 | |
| | RMSE | 63.5153 | RMSE | 72.3797 | |
| | Mean absolute deviation | 44.4785 | Mean absolute deviation | 56.3246 | |
| | –log-likelihood | 50.132 | –log-likelihood | 28.5043 | |
| | SSE | 36307.8 | SSE | 26194.1 | |
| | Sum frequency | 9 | Sum frequency | 5 | |

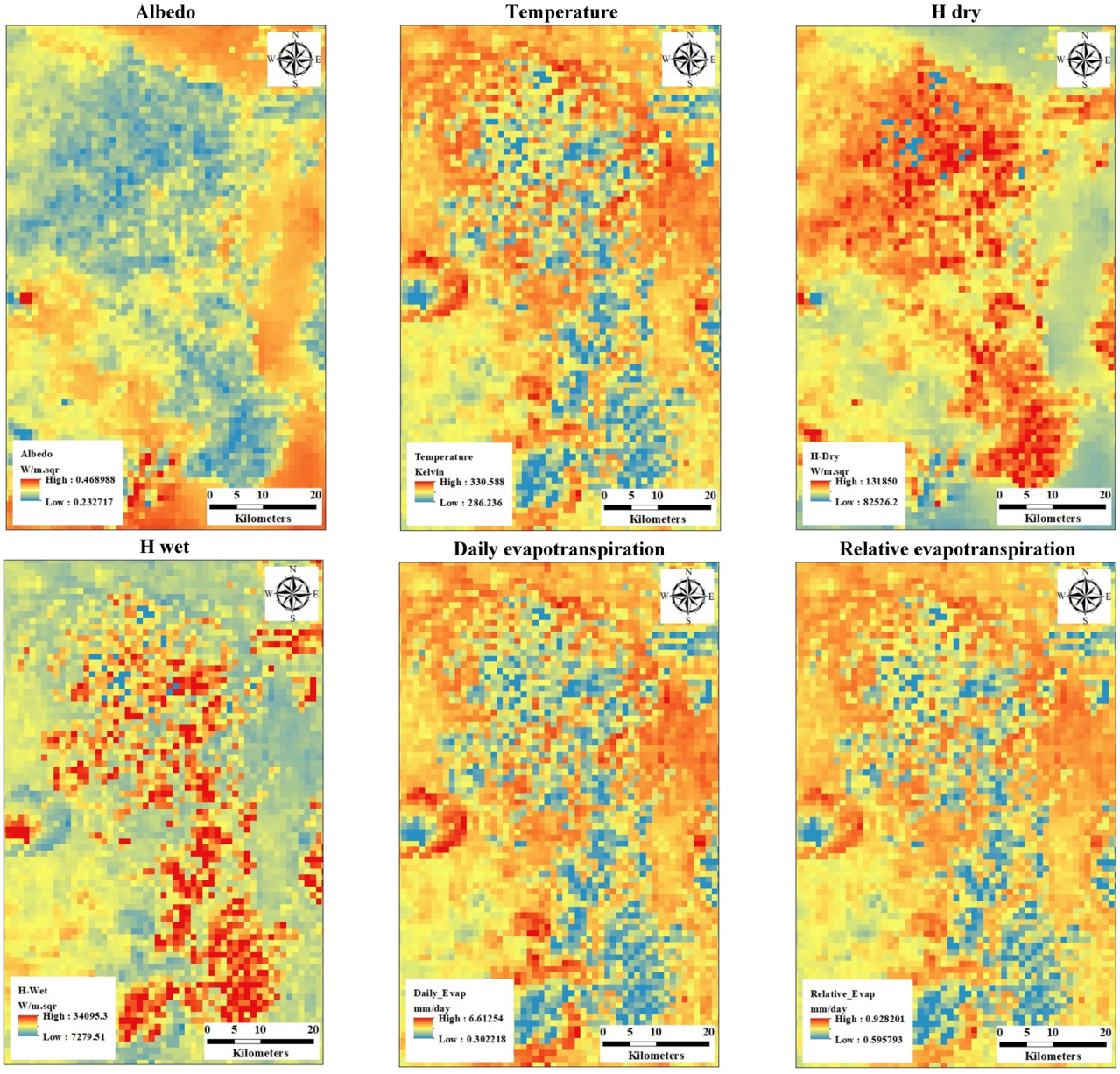


**Figure 7:** SEBS outputs estimated using MERIS and AATSR data.

on SEBS input data. Results show insignificance difference in SEBS input desirability in terms of temperature in general (Figure 6a–c). According to Table 2, –2*log-likelihood values for the maximum, minimum, and average temperatures were estimated to be closer to 83 with marginal variation [53].

Finally, solar radiations in Figure 6f show arbitrary Gaussian behavior with –2*log-likelihood value estimated to be 199.8, which is the highest value among SEBS input parameters. A higher Gaussian value indicates that the role of solar radiation in SEBS daily ET in the Wadi Ad-Dwaser is still understudied [39,54]. Such a correlation needs to be considered in water conservation plants in arid environments [55].

The ANN analysis of a hidden layer, eight nodes, and hyperbolic refraction stimulation function was performed under specific conditions for each temporal dataset. These settings were sensibly practiced to limit the overfitting of the used algorithm, and ANN findings are presented in Table 3.

Based on RMSE and –log-likelihood, the dataset of April showed that relative humidity followed by wind speed was used to descend the neural network classification parameters. The significant variables obtained from the analysis imply their importance to determine their

**Table 4:** The univariate and the quantile analyses of SEBS output thematic maps

| | Daily_Evap | Relative_Evap | Albedo | Temp | *H*-dry | *H*-wet |
|---|---|---|---|---|---|---|
| Minimum | 0.3242 | 0.1997 | 0.1787 | 258.8811 | 42871.4548 | 4355.4284 |
| Maximum | 8.9951 | 0.9532 | 0.7247 | 341.6599 | 131850.2985 | 45843.4828 |
| Mean | 4.6521 | 0.8927 | 0.3533 | 320.6427 | 100361.5447 | 10746.6688 |
| Sigma | 0.5836 | 0.0211 | 0.0502 | 3.3124 | 7818.0457 | 1856.7539 |
| Median | 4.6803 | 0.8944 | 0.3632 | 320.8219 | 98774.0922 | 10432.7801 |
| Coefficient variation | 0.2341 | 0.0402 | 0.2635 | 0.0202 | 0.1602 | 0.5292 |
| P75 threshold | 4.9878 | 0.9002 | 0.3952 | 322.2586 | 104800.7300 | 11405.1564 |
| P80 threshold | 5.0624 | 0.9017 | 0.3973 | 322.5819 | 106224.3915 | 11648.2505 |
| P85 threshold | 5.1556 | 0.9032 | 0.4005 | 323.0670 | 108003.9684 | 11972.3759 |
| P90 threshold | 5.2767 | 0.9061 | 0.4037 | 323.7137 | 111029.2491 | 12539.5954 |
| Maximum error | 0.0093 | 0.0015 | 0.0011 | 0.1617 | 88.9788 | 81.0314 |

influence on the SEBS estimation [44]. Temperature (minimum, average, and maximum, correspondingly) came in second in the significance order, while solar radiation ranked the last. This could be explained due to the close range of the wind speed and the relative humidity variations within the collected data from the different meteorological stations. On the contrary, solar radiation showed the highest range of input data variability [56,57].

According to the Gaussian analysis with −2*log-likelihood value of −6.708327, the wind speed was the least desirably function that affects the SEBS algorithm to conduct the daily ET within the selected study area as shown in Figure 6e [40,58].

The daily ET showed uneven −log-likelihood values with SEBS input parameters integrated together for satisfactory results [59]. Each parameter value was multiplied to its corresponded layer, and then the layers were overlaid all together to be introduced to the final optimization process [55].

## 3.3 Outputs inconsistencies

The spatial distribution of daily ET values varies over Wadi Ad-Dwaser. The extreme daily ET findings are situated at the West and East side of the study area, while in the central region of the Wadi Ad-Dwaser, the daily ET findings are ranged from low to medium. The mean daily ET was estimated to be around 2.4 mm/day, with an extreme value reached to 9 mm/day (Figure 7). The range of the estimated daily ET, evaporative fraction, and other heat fluxes indices is presented in Table 4.

The estimation of the daily ET values was not performed over the agricultural practices of the study area only, and it was also extended over the peripheral bare soils to estimate the potential ET values instead of the actual values. The tendency of the algorithm to estimate the potential ET over noncroplands is the reason behind the higher daily ET values (Table 4). This shift from the mean values of the daily ET was due to the absence of the biological parameters, especially the leaf area index (LAI) found using the MERIS sensor and the daily estimation is based on only the physical parameters found from the AATSR and the meteorological data [10,36].

Following the daily ET mapping, the evaporative fraction was also mapped in along with surface temperature, surface albedo, and the hot and the cold heat fluxes at the TOC level. The coefficient of variation was precisely used in the present study to assess the SEBS output inconsistencies (Table 4). The smallest coefficient was pointed out by the surface temperature (0.02), while the daily ET values and the corresponded albedo values showed robust dependencies of 0.234 and 0.263, respectively.

The performed regression analysis (Table 5) showed two distinctive behaviors of the estimated daily ET and each of the surface temperature and the heat fluxes as shown in Figure 8. The estimated daily ET showed persistent correlation with the surface albedo and the hot heat fluxes, while it was proportionally correlated with the surface temperature and inversely correlated with the cold heat fluxes [15,18,60,61].

**Table 5:** SEBS output regression functions

| | Regression function | $R^2$ |
|---|---|---|
| Daily ET against surface albedo | $0.005X + 1.984$ | 0.43 |
| Daily ET against *H*-dry fluxes | $-0.004X - 1.843$ | 0.42 |
| Daily ET against *H*-wet fluxes | $-2.79 \ln(x) - 3.523$ | 0.89 |
| Daily ET against surface temperature | $2.84 \ln(x) - 3.754$ | 0.88 |

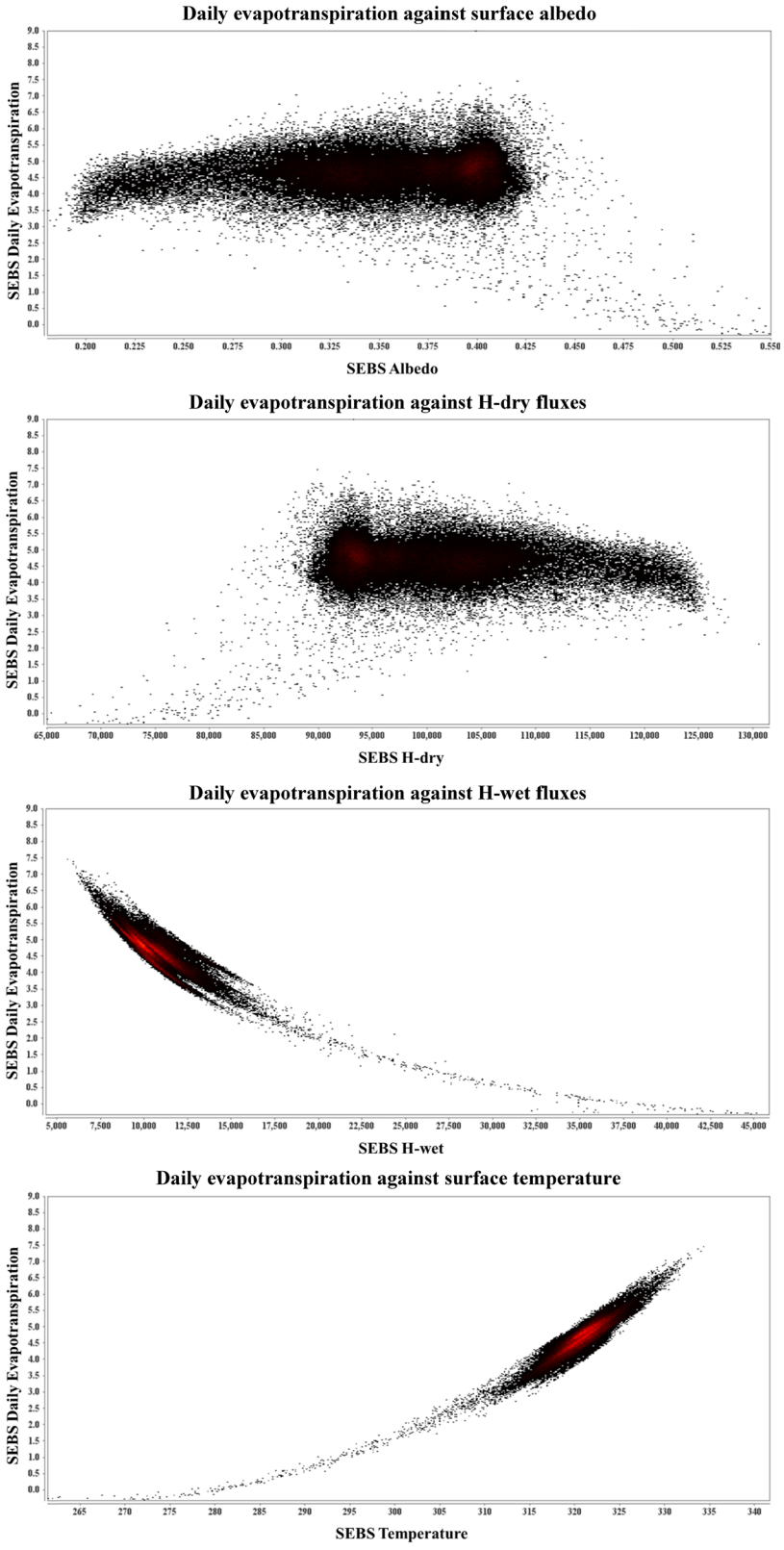


**Figure 8:** SEBS input parameter correlations with the estimated daily evapotranspiration.

The correlation established between the estimated daily ET and either the surface temperature or the cold heat fluxes was logical in principle, and it proves the efficiency of the SEBS model as well as the output intra-relationships [62–64]. Meanwhile, the surface albedo and the hot heat fluxes seemed to be less significant in SEBS output inconsistencies [44,65]. Accordingly, effective water-saving plans shall continuously monitor surface temperature variations to ensure their validity particularly in arid regions where the water resource management plans are always questioned of its sustainability [10,66].

The use of the SEBS input/output inconsistencies is to develop and disseminate information about condition-specific management approaches that are considered to be profitable and practical for agricultural practices and the supply chain [67,68]. The use of the meteorological data for SEBS model performance is to estimate the daily ET on an accurate manner to minimize the overfit of the estimation using a single month data [22,69,70].

# 4 Conclusions

SEBS was used in the arid environments of Wadi Ad-Dwaser to estimate the daily ET. The algorithm estimated daily ET values are within the empirical range of 1.2–8.9 mm/day. The desirability function as well as the ANN analysis show the significant importance of input datasets used to investigate and examine the SEBS input parameters over the designated study area. Temperature and relative humidity are significant parameters and must be considered and regularly monitored for water quality management plans in the selected study area. Further temporal data analysis is required to identify the trend of the solar radiation role. The current investigation is a biophysical evaluation that delivers information that could be used by farmers to enhance their cropping pattern. Furthermore, the outcomes could be valuable for other investigators who could use these results for diverse studies. For future considerations, a greater number of factors such as soil, climate, irrigation facilities, and socioeconomic shall be taken into consideration.

**Acknowledgment:** This project was funded by the Deanship of Scientific Research (DSR), King Abdulaziz University, Jeddah, under grant no. (G-65-155-1440). The authors, therefore, acknowledge with thanks, DSR technical and financial support.

**Conflict of interest:** The author declares that there is no conflict of interest regarding the publication of this article.

# References

[1] Brunet Y, Nunez M, Lagouarde J-P. A simple method for estimating regional evapotranspiration from infrared surface temperature data. ISPRS J Photogramm Remote Sens. 1991;46:311–27.
[2] Zhang Y, Li L, Chen L, Liao Z, Wang Y, Wang B, et al. A modified multi-source parallel model for estimating urban surface evapotranspiration based on ASTER thermal infrared data. Remote Sens. 2017;9:1029.
[3] Peng J, Liu Y, Zhao X, Loew A. A direct algorithm for estimating daily regional Evapotranspiration from modis TOA radiances. 2012 IEEE international geoscience and remote sensing symposium. Munich, Germany: IEEE; 2012. p. 702–5
[4] Montes C, Jacob F. Comparing Landsat-7 ETM + and ASTER Imageries to estimate daily evapotranspiration within a Mediterranean vineyard watershed. IEEE Geosci Remote Sens Lett. 2017;14:459–63.
[5] Sarkkola S, Hökkä H, Koivusalo H, Nieminen M, Ahti E, Päivänen J, et al. Role of tree stand evapotranspiration in maintaining satisfactory drainage conditions in drained peatlands. Can J For Res. 2010;40:1485–96.
[6] Pinnix GD, Miller GL. Comparing evapotranspiration rates of tall fescue and bermudagrass in North Carolina. Agric Water Manag. 2019;223:105725.
[7] Ladson A, Moore I. Soil water prediction on the Konza Prairie by microwave remote sensing and topographic attributes. J Hydrol. 1992;138:385–407.
[8] Sewell PD, Quideau SA, Dyck M, Macdonald E. Long-term effects of harvest on boreal forest soils in relation to a remote sensing-based soil moisture index. For Ecol Manag. 2020;462:117986.
[9] Kustas W, Norman J. Use of remote sensing for evapotranspiration monitoring over land surfaces. Hydrol Sci J. 1996;41:495–516.
[10] Elhag M, Psilovikos A, Manakos I, Perakis K. Application of the SEBS water balance model in estimating daily evapotranspiration and evaporative fraction from remote sensing data over the Nile Delta. Water Resour Manag. 2011;25:2731–42.
[11] Olioso A, Chauki H, Courault D, Wigneron J-P. Estimation of evapotranspiration and photosynthesis by assimilation of remote sensing data into SVAT models. Remote Sens Environ. 1999;68:341–56.
[12] Wu C-D, Cheng C-C, Lo H-C, Chen Y-K. Application of SEBAL and Markov models for future stream flow simulation through remote sensing. Water Resour Manag. 2010;24:3773–97.
[13] Hartman MD, Baron JS, Ojima DS. Application of a coupled ecosystem-chemical equilibrium model, DayCent-Chem, to stream and soil chemistry in a Rocky Mountain watershed. Ecol Model. 2007;200:493–510.
[14] Johnson NL, Kotz S, Balakrishnan N. Continuous univariate distributions, vol. 2 of wiley series in probability and

mathematical statistics: applied probability and statistics. New York: Wiley; 1995.
[15] Shahzad Sultan IA. Determination of daily regional scale actual evapotranspiration for indus sub-basin using landsat ETM. Pak J Meteorol. 2008;4:49–58.
[16] Krishnan N, Raj C, Chaubey I, Sudheer K. Parameter estimation of SWAT and quantification of consequent confidence bands of model simulations. Environ Earth Sci. 2018;77:470.
[17] Roerink G, Su Z, Menenti M. S-SEBI: a simple remote sensing algorithm to estimate the surface energy balance. Phys Chem Earth Part B Hydrol Ocean Atmosphere. 2000;25:147–57.
[18] Su Z. The surface energy balance system (SEBS) for estimation of turbulent heat fluxes. Hydrol Earth Syst Sci. 2002;6:85–99.
[19] Su H, McCabe M, Wood EF, Su Z, Prueger J. Modeling evapotranspiration during SMACEX: comparing two approaches for local-and regional-scale prediction. J Hydrometeorol. 2005;6:910–22.
[20] Chen X, Su Z, Ma Y, Yang K, Wang B. Estimation of surface energy fluxes under complex terrain of Mt. Qomolangma over the Tibetan Plateau. Hydrol Earth Syst Sci. 2013;17:1607–18.
[21] Su Z. The surface energy balance system (SEBS) for estimation of turbulent heat fluxes. HESS. 2002;6(1):85–100.
[22] Allen RG, Tasumi M, Trezza R. Satellite-based energy balance for mapping evapotranspiration with internalized calibration (METRIC) – model. J Irrig Drain Eng. 2007;133:380–94.
[23] Derringer G, Suich R. Simultaneous optimization of several response variables. J Qual Technol. 1980;12:214–9.
[24] Ficici F, Koksal S, Karacadag MC. Optimization of cutting parameters for surface roughness of stainless steel in drilling process. Int J Adv Sci. 2012;2:114–21.
[25] Kunnan AJ, Carr NT. Statistical analysis of test results. The encyclopedia of applied linguistics. New Jersey, USA: John Wiley & Sons; 2013.
[26] Sibalija TV, Majstorovic VD. An integrated approach to optimise parameter design of multi-response processes based on Taguchi method and artificial intelligence. J Intell Manuf. 2012;23:1511–28.
[27] Muthukrishnan N, Babu TM, Ramanujam R. Fabrication and turning of Al/SiC/B4C hybrid metal matrix composites optimization using desirability analysis. J Chin Inst Ind Eng. 2012;29:515–25.
[28] Maiyar LM, Ramanujam R, Venkatesan K, Jerald J. Optimization of machining parameters for end milling of Inconel 718 super alloy using Taguchi based grey relational analysis. Proc Eng. 2013;64:1276–82.
[29] Jo S, Sung H, Ahn B. A comparative study on the performance of intrusion detection using decision tree and artificial neural network models. J Soc Korea Ind Syst. 2015;11:33–45.
[30] Lipton ZC, Berkowitz J, Elkan C. A critical review of recurrent neural networks for sequence learning. arXiv preprint arXiv:150600019. 2015.
[31] Lek S, Guégan J-F. Artificial neuronal networks: application to ecology and evolution. Berlin, Germany: Springer Science & Business Media; 2012.
[32] Abyaneh HZ. Evaluation of multivariate linear regression and artificial neural networks in prediction of water quality parameters. J Environ Health Sci Eng. 2014;12:40.
[33] Vafakhah M. Application of artificial neural networks and adaptive neuro-fuzzy inference system models to short-term streamflow forecasting. Can J Civ Eng. 2012;39:402–14.
[34] Yilmaz N, Elhag M, Yasar U. Consideration of phytoplankton composition and water quality of Anamur (Dragon) Creek, Turkey. Desalin Water Treat. 2017;91:386–94.
[35] Wen X, Fang J, Diao M, Zhang C. Artificial neural network modeling of dissolved oxygen in the Heihe river, Northwestern China. Environ Monit Assess. 2013;185:4361–71.
[36] Elhag M, Bahrawi JA. Realization of daily evapotranspiration in arid ecosystems based on remote sensing techniques. geoscientific instrumentation. Methods Data Syst. 2017;6:141.
[37] Elhag M, Bahrawi JA. Conservational use of remote sensing techniques for a novel rainwater harvesting in arid environment. Environ Earth Sci. 2014;72:4995–5005.
[38] Almazroui M. Simulation of present and future climate of Saudi Arabia using a regional climate model (PRECIS). Int J Climatol. 2013;33:2247–59.
[39] Elhag M. Evaluation of different soil salinity mapping using remote sensing techniques in arid ecosystems, Saudi Arabia. J Sens. 2016;2016:7596175–84.
[40] Psilovikos A, Elhag M. Forecasting of remotely sensed daily evapotranspiration data over Nile Delta region, Egypt. Water Resour Manag. 2013;27:4115–30.
[41] Liu C, Wang H. The interface processes of water movement in the soil-crop-atmosphere system and water-saving regulation. Beijing: Science Press; 1999.
[42] Taylor AR. A method for surface irrigation design based on infiltration using the border strip as an infiltrometer: Lincoln College. Christchurch, New Zealand: University of Canterbury; 1981.
[43] Monahan AH. Nonlinear principal component analysis by neural networks: theory and application to the Lorenz system. J Clim. 2000;13:821–35.
[44] Elhag M. Inconsistencies of SEBS model output based on the model inputs: global sensitivity contemplations. J Indian Soc Remote. 2016;44:435–42.
[45] Cheng C, Parzen E. Unified estimators of smooth quantile and quantile density functions. J Stat Plan Inference. 1997;59:291–307.
[46] Robert CP, Gene Hwang J. Maximum likelihood estimation under order restrictions by the prior feedback method. J Am Stat Assoc. 1996;91:167–72.
[47] Saaty TL. A scaling method for priorities in hierarchical structures. J Math Psychol. 1977;15:234–81.
[48] Yager RR. On ordered weighted averaging aggregation operators in multicriteria decisionmaking. IEEE Trans Syst Man Cybern. 1988;18:183–90.
[49] Hajkowicz SA, McDonald GT, Smith PN. An evaluation of multiple objective decision support weighting techniques in natural resource management. J Environ Plan Manag. 2000;43:505–18.
[50] Su Z, Yacob A, Wen J, Roerink G, He Y, Gao B, et al. Assessing relative soil moisture with remote sensing data: theory, experimental validation, and application to drought monitoring over the North China Plain. Phys Chem Earth Parts A/B/C. 2003;28:89–101.
[51] Li F, Kustas WP, Prueger JH, Neale CM, Jackson TJ. Utility of remote sensing–based two-source energy balance model under low-and high-vegetation cover conditions. J Hydrometeorol. 2005;6:878–91.
[52] Li Z-L, Tang R, Wan Z, Bi Y, Zhou C, Tang B, et al. A review of current methodologies for regional evapotranspiration estimation from remotely sensed data. Sensors. 2009;9:3801–53.

[53] Singh A, Datta S, Mahapatra SS. Principal component analysis and fuzzy embedded Taguchi approach for multi-response optimisation in machining of GFRP polyester composites: a case study. Int J Ind Syst Eng. 2013;14:175–206.
[54] Elhag M. Remotely sensed vegetation indices and spatial decision support system for better water consumption regime in Nile delta. A case study for rice cultivation suitability map. J Life Sci. 2014;11:201–9.
[55] Pettorelli N, Vik JO, Mysterud A, Gaillard J-M, Tucker CJ, Stenseth NC. Using the satellite-derived NDVI to assess ecological responses to environmental change. Trends Ecol Evol. 2005;20:503–10.
[56] Bastawesy ME. Ramadan Ali R, Faid A, Osta ME. Assessment of waterlogging in agricultural megaprojects in the closed drainage basins of the western desert of Egypt. Hydrol Earth Syst Sci. 2013;17:1493–501.
[57] Jia K, Liang S, Gu X, Baret F, Wei X, Wang X, et al. Fractional vegetation cover estimation algorithm for Chinese GF-1 wide field view data. Remote Sens Environ. 2016;177:184–91.
[58] Dureja J, Gupta V, Sharma VS, Dogra M, Bhatti MS. A review of empirical modeling techniques to optimize machining parameters for hard turning applications. Proc Inst Mech Eng B J Eng Manuf. 2016;230:389–404.
[59] Glenn EP, Huete AR, Nagler PL, Nelson SG. Relationship between remotely-sensed vegetation indices, canopy attributes and plant physiological processes: what vegetation indices can and cannot tell us about the landscape. Sensors. 2008;8:2136–60.
[60] Su Z, Schmugge T, Kustas W, Massman W. An evaluation of two models for estimation of the roughness height for heat transfer between the land surface and the atmosphere. J Appl Meteorol. 2001;40:1933–51.
[61] Chen K-S, Wu T-D, Tsang L, Li Q, Shi J, Fung AK. Emission of rough surfaces calculated by the integral equation method with comparison to three-dimensional moment method simulations. IEEE Trans Geosci Remote Sens. 2003;41:90–101.
[62] Cleugh HA, Leuning R, Mu Q, Running SW. Regional evaporation estimates from flux tower and MODIS satellite data. Remote Sens Environ. 2007;106:285–304.
[63] Vinukollu RK, Wood EF, Ferguson CR, Fisher JB. Global estimates of evapotranspiration for climate studies using multi-sensor remote sensing data: evaluation of three process-based approaches. Remote Sens Environ. 2011;115:801–23.
[64] McColl KA, Salvucci GD, Gentine P. Surface flux equilibrium theory explains an empirical estimate of water-limited daily evapotranspiration. J Adv Model Earth Syst. 2019;11:2036–49.
[65] Timmermans WJ, Gieske AS, Kustas WP, Wolski P, Arneth A, Parodi GN. Determination of water and heat fluxes with MODIS imagery. In: Maun B, editor. Remote sensing for agriculture, ecosystems, and hydrology V. California, USA: International Society for Optics and Photonics; 2004. p. 444–55.
[66] Rice B, Harter T, Foglia L, Kisekka I. Automated Basin-wide ET estimation using the SEBS method to improve groundwater sustainability plan development. AGUFM. 2019;2019:H21C-08.
[67] Kumar V, Panu U. Predictive assessment of severity of agricultural droughts based on agro-climatic factors 1. J Am Water Resour Assoc. 1997;33:1255–64.
[68] Mandal D, Ghosh PP, Dasgupta M. Appropriate precision agriculture with site-specific cropping system management for marginal and small farmers. Plant Sci Rev. 2012;2013:121.
[69] Allen RG, Jensen ME, Wright JL, Burman RD. Operational estimates of reference evapotranspiration. Agron J. 1989;81:650–62.
[70] Norman L, Tallent-Halsell N, Labiosa W, Weber M, McCoy A, Hirschboeck K, et al. Developing an ecosystem services online decision support tool to assess the impacts of climate change and urban growth in the Santa Cruz watershed; where we live, work, and play. Sustainability. 2010;2:2044–69.